Lateral Electron Confinement with Open Boundaries: Quantum Well States above Nanocavities at Pb(111)

M. Müller,[1,*] N. Néel,[1] S. Crampin,[2,†] and J. Kröger[1]
[1]*Institut für Physik, Technische Universität Ilmenau, D-98693 Ilmenau, Germany*
[2]*Department of Physics, University of Bath, Bath BA2 7AY, United Kingdom*
(Received 10 June 2016; published 22 September 2016)

We have studied electron states present at the Pb(111) surface above Ar-filled nanocavities created by ion beam irradiation and annealing. Vertical confinement between the parallel crystal and nanocavity surfaces creates a series of quantum well state subbands. Differential conductance data measured by scanning tunneling spectroscopy contain a characteristic spectroscopic fine structure within the highest occupied subband, revealing additional quantization. Unexpectedly, reflection at the open boundary where the thin Pb film recovers its bulk thickness gives rise to the lateral confinement of electrons.

DOI: 10.1103/PhysRevLett.117.136803

Electrons confined to structures with dimensions comparable to their de Broglie wavelength exhibit quantization, which is a fundamental aspect of quantum systems. Striking examples are whispering gallery modes in oligothiophene nanorings [1] and in graphene [2] and linear molecules acting as one-dimensional resonators confining nearly free electrons [3,4]. Electron confinement finds application in technological devices including high-brightness light-emitting diodes, semiconductor lasers, photovoltaics, and spintronics [5–7]. At surfaces, quantized states associated with vertical confinement in ultrathin films affect crystal growth [8] and provide a means to monitor film quality [9] and influence chemical reactivity [10] and electron correlations, such as the Kondo effect of molecules [11] and atoms [12].

Lateral electron confinement has been observed in a diverse set of systems with scanning tunneling spectroscopy enabling real-space imaging of quantized states. Examples include states laterally confined to adsorbed metallic quantum dots [13], graphene nanostructures [14–19], atomic chains on metallic surfaces [20], and dangling bond states on semiconductors [21]. The confinement of noble-metal Shockley surface states to, e.g., artificially fabricated atom corrals [22], terraces [23,24], islands [25], magnetic structures [26], and nanopyramids [27], has attracted particular interest, enabling exotic quantum phenomena [28] as well as quasiparticle lifetimes [27,29–33] to be explored.

Confinement in these and related systems is effected by an abrupt change in the potential experienced by electrons, such as the potential rise at the metal-vacuum boundary at chain, step, and island edges, or the adatom potential at artificially fabricated corrals [34], while confinement due to the magnetic vector potential is well known in semiconductor quantum dots [35]. Here, we use artificially engineered buried lattice defects of a Pb(111) crystal, in the form of Ar-filled voids located just beneath the crystal surface [Fig. 1(a)] to both vertically *and* laterally confine Pb conduction electrons. The vertical confinement is conventionally realized by the potential rise at the Pb(111)-vacuum and the Pb bulk-void interface and leads to a main series of quantum well states [Fig. 1(b)] as previously reported at Al(111) [36]. In addition, we achieve further quantization due to electron reflection at the *open* boundary where the thin Pb film recovers its bulk thickness. Lateral confinement is therefore induced by the removal of vertical confinement, representing a hitherto unexplored mechanism for electron confinement. We support our experimental findings using a semianalytic model accounting for the main features and discuss the role of elastic and inelastic scattering on the confined electron lifetimes.

Experiments were performed with a scanning tunneling microscope (STM) operated in ultrahigh vacuum (10^{-9} Pa) and at low temperature (6 K). Atomically clean Pb(111) was obtained by repeated Ar^+ bombardment and annealing. To efficiently create subsurface voids, the ion kinetic energy and current density at the sample were set to 1.1 keV and 5 μA cm^{-2}, respectively, with the ion beam impinging onto the surface at an angle of 30° with respect to the surface normal. Samples were subsequently annealed at 560 K for 20 min. All STM images were recorded at constant current with the bias voltage applied to the sample. Spectra of the differential conductance (dI/dV) were acquired by modulating the sample voltage (5 mV_{pp}, 6.3 kHz) and detecting the current response with a lock-in amplifier.

STM images of the prepared surface confirm the presence of Ar-filled subsurface cavities [Fig. 1(a)] with cross sectional diameters in the 2.5–7 nm range, as previously reported at Al, Cu, and Ag surfaces [36–40], and which result from the diffusion and aggregation during annealing of implanted Ar, most likely as Ar+vacancy complexes [41]. Spectra of dI/dV acquired atop their centers contain considerable structure [Fig. 1(b)] attributable to quantum well states (QWS) associated with the vertical confinement of electrons between the surfaces of the buried cavity and the crystalline sample. Calculations

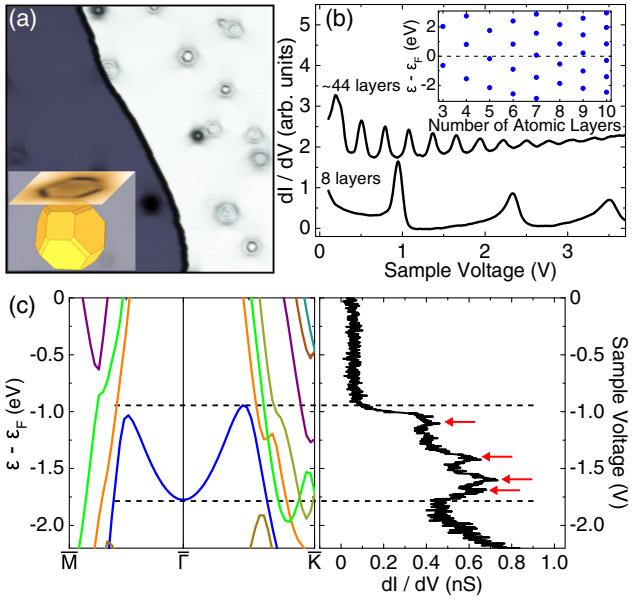

FIG. 1. (a) STM image of Pb(111) showing buried cavities on a lower (dark gray) and an upper (light gray) terrace (0.5 nA, 1.08 V, 94 nm × 94 nm). Inset: Schematic illustration of a subsurface nanocavity, with geometry based upon Wulff construction using (111), (110), and (001) Pb surface energies. (b) Constant-current (0.5 nA) dI/dV spectra (vertically offset) acquired atop cavities located at different depths, exhibiting signatures of unoccupied QWS. Inset: Calculated QWS energies as a function of the Pb layer thickness. (c) Left: Calculated energy band structure of a four-layer Pb(111) thin film showing the dispersion of the highest occupied QWS (blue line) with a 0.2 eV energy shift applied to align band minimum. Right: Experimental constant-height dI/dV spectrum acquired atop the center of a subsurface cavity identified as being four layers below the surface, showing spectroscopic fine structure (red arrows) within the band of the highest occupied QWS (feedback loop parameters: 1 nA and −2.5 V).

of QWS energies within thin Pb films show a distinctive thickness dependence. Based upon a comparison with QWS energies found using density functional theory [inset in Fig. 1(b)], we have been able to identify the depth of individual nanocavities. As a result, we find that our preparation method yields a preponderance of cavities buried four, six, and eight layers below the surface. A preference for thin Pb overlayers to form with certain thicknesses was reported previously for thin films on Cu [42] and Si [43] and attributed to a quantum size effect. An increased separation between the QWS and the Fermi level can be observed with a bilayer periodicity, which can explain the preference of an even number of layers in our system.

The QWS dispersion parallel to the surface in thin Pb films is parabolic near the Brillouin zone center $\bar{\Gamma}$ but, due to hybridization, flattens and disperses downward for larger wave vector k. As an example, Fig. 1(c) shows the dispersion of the highest occupied QWS (HOQWS) for a four-layer Pb(111) film as a blue line. The hybridization effects increase (and consequently the effective mass) for higher QWS energies, leading to states at ≈1 eV above the Fermi level ε_F and higher having a very narrow line shape in dI/dV spectra. However, occupied states exhibit an identifiable bandwidth [44], and close inspection of dI/dV spectra recorded atop the center of cavities reveal additional structure within the bandwidth of the HOQWS, in the form of a series of peaks [indicated by horizontal arrows in the right panel of Fig. 1(c)] whose location varies with the diameter of the particular subsurface cavity. This structure manifests the existence of additional quantization of the electron states, which we associate with *lateral* confinement to the region between the cavity and the Pb surface.

We base this unusual interpretation of the fine structure in the HOQWS on the model illustrated in the inset in Fig. 2, comprising a circularly symmetric cavity of radius R a depth L beneath the surface ($z = 0$), with side facets normal to the upper face extending into the bulk ($z \to -\infty$). Electrons are ideally excluded from the volume of the cavity and the vacuum region outside the crystal while being free to move within the region occupied by Pb; there we set the potential to zero, since the relevant Pb states disperse with effective mass m^* close to the free-electron mass m, both normal and parallel to the surface. We find the local density of states (DOS) at energy ε as $\rho(\mathbf{r};\varepsilon) = 1/\pi \mathrm{Im} G(\mathbf{r},\mathbf{r};\varepsilon)$, where the Green function G satisfies the inhomogeneous Schrödinger equation $(\mathcal{H}-\varepsilon)G = \delta(\mathbf{r}-\mathbf{r}')$. We include in the Hamiltonian $\mathcal{H} = -\hbar^2/(2m)\nabla^2 + V - i\Sigma_i(\varepsilon)$ a non-Hermitian self-energy term accounting for inelastic lifetime effects, for which

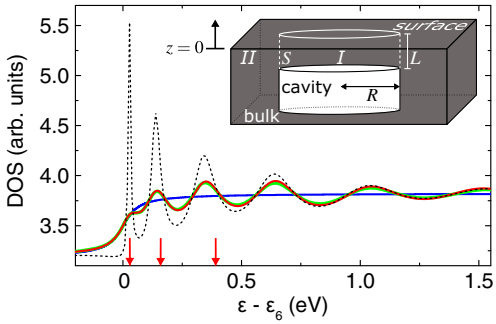

FIG. 2. Density of states (DOS) of the HOQWS for a four-layer Pb film (blue line) integrated over film thickness and atop a 2.7 nm radius bubble four layers beneath the surface omitting (red line) and including (green line) interband scattering. The dashed line shows the DOS in the absence of inelastic lifetime broadening ($\Sigma_i = 0$). The arrows in the main figure indicate the expected energies of electrons ideally confined to region I. Inset: Model geometry and partitioning of space used in calculations. The cavity with radius R exhibits a surface-vacuum distance L. Electrons are excluded from the cavity and the vacuum above the surface. Surface S separates region I, the space between the cavity and the crystal surface, from region II, where the electron is no longer confined in the vertical (downwards) direction.

we use $\Sigma_i = \Sigma_{\text{e-ph}} + \Sigma_{\text{e-e}}$ with electron-phonon and electron-electron interaction terms $\Sigma_{\text{e-ph}} = 12$ meV and $\Sigma_{\text{e-e}} = \alpha(\varepsilon - \varepsilon_F)^2$, respectively, with $\alpha = 0.012$ eV^{-1} from measured values in Pb overlayers [44,45]. If the cavity has an infinite extent ($R \to \infty$), then integrating over the well width L the DOS associated with the nth quantum well subband is $\rho_n^{\infty}(\varepsilon) = m/(2\pi^2\hbar^2)(\pi - \arg[\varepsilon - \varepsilon_n + i\Sigma_i(\varepsilon)])$, corresponding to a lifetime-broadened steplike increase at the threshold QWS energy $\varepsilon_n = \hbar^2 n^2 \pi^2/(2mL^2)$ (blue curve in Fig. 2).

For a cavity of finite radius we partition space into regions I and II, shown in the inset in Fig. 2, separated by surface S. Working in I alone, the Green function satisfies the inhomogeneous Schrödinger equation with embedded Hamiltonian [46] $\mathcal{H}_{\Sigma_S} = \mathcal{H} + \hbar^2/(2m)\delta(\mathbf{r} - \mathbf{r}_S)\mathbf{n}_S \cdot \nabla + \Sigma_S(\varepsilon)$ ($\mathbf{n}_S$, surface normal pointing from I to II), where together the second term and surface operator $\Sigma_S(\varepsilon) = \delta(\mathbf{r} - \mathbf{r}_S)\delta(\mathbf{r}' - \mathbf{r}'_S)\Sigma_S(\mathbf{r}_S, \mathbf{r}'_S; \varepsilon)$ ensure that the Green function in I matches correctly on S to the Green function in II. The embedding potential Σ_S found from $\mathbf{n}_S \cdot \nabla\psi = -2m/\hbar^2 \int_S \Sigma_S \psi dS'$ for $\mathbf{r} \in S$, where ψ is the solution of the Schrödinger equation in region II at energy ε, is

$$\Sigma_S(\mathbf{r}_S, \mathbf{r}'_S; \varepsilon) = -\frac{\hbar^2}{2m\pi^2 R}\sum_M e^{iM(\phi-\phi')}\int_0^{\infty} dq \sin(qz)\sin(qz') \times \frac{d}{dr}\ln\left[H_M^{(1)}\left(\sqrt{2m\varepsilon/\hbar^2 - q^2}\, r\right)\right]\Bigg|_{r=R}, \quad (1)$$

with $H_M^{(1)}$ the Hankel function and M the angular momentum quantum number. Finally, expanding the Green function in region I as

$$G(\mathbf{r}, \mathbf{r}'; \varepsilon) = \frac{1}{\pi L}\sum_M e^{iM(\phi-\phi')}\sum_{n,n'>0}\sin(k_n z)\sin(k_{n'} z') \times \mathcal{G}_{M,n,n'}(r, r', \varepsilon) \quad (2)$$

with $k_n = n\pi/L$, we solve for $\mathcal{G}$. Further analytic development is possible upon neglecting interband coupling, i.e., the mixing of states with different n, n'. The virtual coincidence of numerical results obtained by omitting (red curve in Fig. 2) and including (green curve in Fig. 2) interband coupling validates this approximation. Within this approximation, the DOS from the nth QWS subband integrated over the well width L above the center of the cavity ($r = 0$, whence only states with $M = 0$ contribute) is $\rho_n(\varepsilon) = \rho_n^{\infty}(\varepsilon) + m/(2\pi\hbar^2)\text{Re}(2\mathcal{R}_n(\varepsilon)/[1 - \mathcal{R}_n(\varepsilon)])$, where

$$\mathcal{R}_n(\varepsilon) = \frac{H_0^{(1)\prime}(\kappa_n r) - \mathcal{L}_n(\varepsilon)H_0^{(1)}(\kappa_n r)}{\mathcal{L}_n(\varepsilon)H_0^{(2)}(\kappa_n r) - H_0^{(2)\prime}(\kappa_n r)}\Bigg|_{r=R}, \quad (3)$$

with the prime denoting d/dr, $\kappa_n = \sqrt{2m\epsilon/\hbar^2 - k_n^2}$, and

$$\mathcal{L}_n(\epsilon) = \int_0^{\infty} dq \frac{4k_n^2}{\pi L}\frac{\sin^2(qL)}{(q^2 - k_n^2)^2} \times \frac{d}{dr}\ln\left[H_0^{(1)}\left(\sqrt{2m\epsilon/\hbar^2 - q^2}\, r\right)\right]\Bigg|_{r=R}. \quad (4)$$

This DOS is precisely equivalent to that of a system in which electrons are free to move in two dimensions within a circular domain, with $\mathcal{R}_n$ an effective reflection coefficient whereby an outgoing radial circular wave $H_0^{(1)}(\kappa_n r)$ results in the incoming wave $\mathcal{R}_n(\varepsilon)H_0^{(2)}(\kappa_n r)$ following reflection at boundary radius R. Here the reflection is not caused by a conventional confining potential but by the *removal* beyond R of the confinement in the perpendicular direction, with $\mathcal{R}_n$ vanishing if the electron remains confined to a depth L in region II. In effect, the electron is reflected by the "open door" that exists beyond the cavity, should it attempt to move deeper into the crystal.

The consequences of this reflection and concomitant confinement are visible in the calculated DOS of the QWS subband, with Fig. 2 showing the energy variation using parameters appropriate to the HOQWS of a four-layer Pb film above a cavity with $R = 2.7$ nm. There is good correspondence between the features exhibited by the DOS and the structure observed in the measured dI/dV spectra recorded atop subsurface cavities [Fig. 1(c)]. In particular, the steplike increase characteristic of the thin film ($R \to \infty$) is replaced by a series of quantized resonant levels, this being especially apparent if the effects of inelastic lifetime broadening processes are suppressed in the calculations ($\Sigma_i = 0$; dashed line in Fig. 2). Further measured and calculated spectra are presented in Fig. 3 for different cavity depths and sizes, along with the range of energies for which the HOQWS exhibits parabolic dispersion—above this, the model is no longer applicable. It is worth noting that we have confirmed using similar methods to those in Ref. [48] that additional low-amplitude peaks present in the experimental dI/dV spectra (arrows in Fig. 3) are consistent with expected contributions from lower symmetry states at slightly off-center locations in domains with C_{3v} symmetry, appropriate to the (111) faces of the polyhedral cavities given by the Wulff construction.

The resonances in calculated spectra can be identified with poles in the Green function that occur when $\mathcal{R}_n(\varepsilon) = 1$, which requires $d/dr \ln J_0(\kappa_n r)|_{r=R} = \mathcal{L}_n(\varepsilon)$. Using asymptotic forms, this becomes $\tan(\kappa_n R - \pi/4) = -\mathcal{L}_n(\varepsilon)/\kappa_n$. Numerically, we find $\text{Re}\mathcal{L}_n(\varepsilon) < 0$, slowly varying and only weakly dependent upon R. Then with $\kappa_n \to 0$ as $\varepsilon \to \varepsilon_n$ from above, the lowest energy resonances correspond closely to the positive asymptotes of the tangent, occurring when $\kappa_n R - \pi/4 \simeq \pi/2, 3\pi/2, \ldots$, or equivalently at energies close to

$$\varepsilon - \varepsilon_n = \frac{\hbar^2(3\pi/4)^2}{2mR^2}, \frac{\hbar^2(7\pi/4)^2}{2mR^2}, \cdots. \quad (5)$$

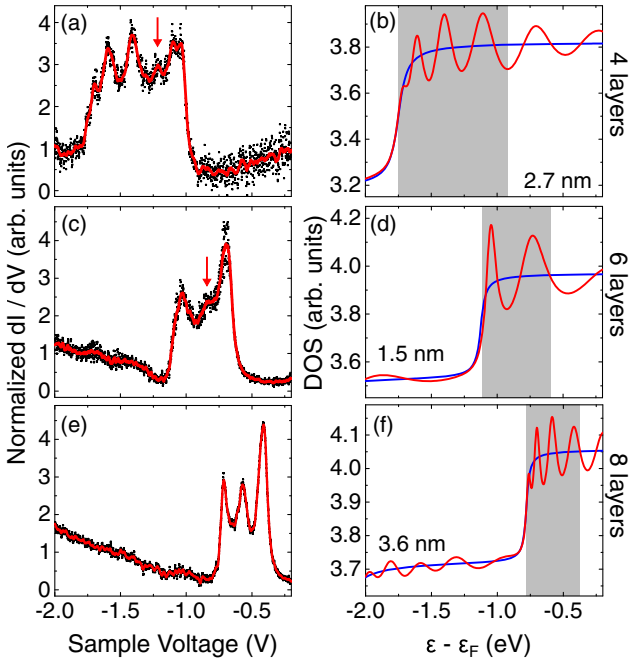

FIG. 3. (a),(c),(e) Experimental dI/dV spectra [feedback loop parameters, 1 nA and −2.5 V (a) or −2 V (c),(e)]. The data were normalized [47] to ensure an improved approximation to the DOS. Arrows in (a) and (c) indicate additional spectroscopic features caused by the reduced symmetry of the (111) facets. (b), (d),(f) Calculated DOS of the HOQWS atop cavities of indicated radii and depths. Shaded areas in (b),(d),(f) show the range of energies with parabolic HOQWS dispersion.

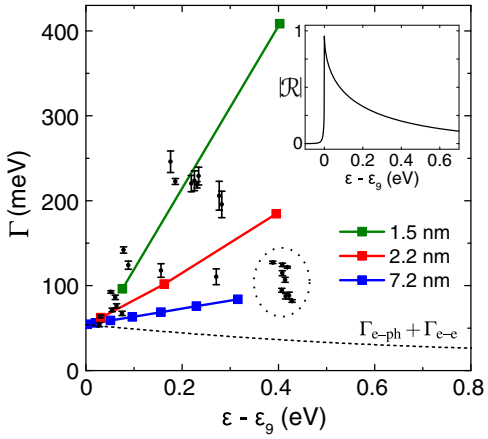

FIG. 4. Experimentally determined (dots) and calculated (squares) linewidths Γ of laterally confined QWS electrons associated with a six-layer deep cavity as a function of energy. The energy is referenced to the onset energy ε_9 of the HOQWS. Calculations were performed for the indicated cavity radii and represent the sum of inelastic ($\Gamma_{\text{e-ph}} + \Gamma_{\text{e-e}}$, dashed line) and elastic contributions to Γ. Experimental data were obtained for cavity radii ranging between 1.5 and 2.2 nm. The data encircled by a dotted line are linewidths of confined states with energies close to the flat region of the HOQWS band. Uncertainty margins represent the statistical uncertainty of the fit procedure. Inset: Calculated energy dependence of the reflection coefficient $|\mathcal{R}|$ at the boundary above a cavity with 2.5 nm radius.

These are the same energies that would arise for hard-wall reflection at the cavity edge, indicating that the open boundary acts as an effective confining barrier. These values are indicated in Fig. 2 as arrows. For higher-order members of the series, the increase in κ_n means the actual value of the logarithmic derivative $\mathcal{L}_n(\varepsilon)$ becomes more important. The resonance energies, therefore, occur increasingly below these values (compare the position of arrows and maxima of red, green, and dashed curves in Fig. 2).

The finite resonance widths Γ (full width at half maximum, FWHM) also signal that confinement due to reflection at the open boundary is not ideal, with electrons persisting in the states only for time $\tau = \hbar/\Gamma$. We observe that there is a crossover between states at lower energies for which the lifetime is limited by intrinsic inelastic effects (e-ph and e-e scattering) to states at higher energies for which passage through the open boundary and escape into the Pb bulk is limiting. The elastic decay rate for electrons at the center of a circular domain of radius R is $\Gamma_e/\hbar \simeq v_g/(2R)(1-|\mathcal{R}|^2)$ with $v_g/(2R)$ the boundary collision rate and $1-|\mathcal{R}|^2$ the escape probability per attempt. Here the group velocity $v_g = \sqrt{2(\varepsilon-\varepsilon_n)/m}$ for parabolic dispersion, and $\mathcal{R}$ is given by Eq. (3). Figure 4 displays total linewidths, Γ, of laterally confined QWS ($\Gamma = \Gamma_i + \Gamma_e$, $\Gamma_i = \Gamma_{\text{e-ph}} + \Gamma_{\text{e-e}}$) from calculated DOS (squares) and experimental dI/dV spectra (dots), which are related to decay rates via $1/\tau = \Gamma/\hbar$. The calculated data show how elastic decay rates become increasingly suppressed as the electron energy approaches, from above, the threshold QWS energy. This is a direct consequence of the decreasing electron velocity impacting upon the collision rate but also of an increasing reflection probability, as pointed to by the near-linear rather than square-root energy variation in Γ. The inset in Fig. 4 shows how $|\mathcal{R}|$ tends to unity as the increasing lateral de Broglie wavelength of the near-threshold electrons increases sensitivity to the change in the environment at the cavity edge.

Experimentally, the FWHM of the laterally confined QWS electrons was extracted by fitting a superposition of Lorentzians and linear background to dI/dV data acquired above six-layer deep cavities with radii between 1.5 and 2.2 nm. The measured linewidths are broadly consistent with the range of calculated values at lower energies but peak approximately 0.2–0.25 eV above the HOQWS onset and then decrease. A cluster of values, encircled in Fig. 4, that deviate noticeably from the calculated values occur at energies close to the upper edge of the HOQWS band [see Fig. 1(c), left panel for the four-layer case], where v_g—and thus Γ—decrease in a manner not described by our model.

In conclusion, we have identified through spectroscopic fine structure unexpected additional electronic state quantization atop near-surface cavities at Pb(111). This unprecedented experimental observation is understood to

originate from reflection at the open boundary where the thin Pb film recovers its bulk thickness and which serves to further isolate electrons parallel to the surface. We present a model that accounts for this phenomenon and quantifies aspects of this hitherto unexplored mechanism for electron confinement. Besides potential applications exploiting the cavity size and depth dependence of the confined electron energy levels for future studies of lifetime physics, we expect similar strong electron scattering at open boundaries will occur more generally in systems where electrons exhibit long wavelengths compared to constriction sizes, with beyond Pb other simple metals and semiconductors most likely to provide examples.

Financial support by the Carl Zeiss Foundation is acknowledged.

*mueller.m@tu-ilmenau.de
†s.crampin@bath.ac.uk

[1] G. Reecht, H. Bulou, F. Scheurer, V. Speisser, B. Carrière, F. Mathevet, and G. Schull, Phys. Rev. Lett. **110**, 056802 (2013).
[2] Y. Zhao, J. Wyrick, F. D. Natterer, J. F. Rodriguez-Nieva, C. Lewandowski, K. Watanabe, T. Taniguchi, L. S. Levitov, N. B. Zhitenev, and J. A. Stroscio, Science **348**, 672 (2015).
[3] J. Repp, P. Liljeroth, and G. Meyer, Nat. Phys. **6**, 975 (2010).
[4] S. Wang, W. Wang, and N. Lin, Phys. Rev. Lett. **106**, 206803 (2011).
[5] Z. Q. Qiu and N. V. Smith, J. Phys. Condens. Matter **14**, R169 (2002).
[6] S. M. Sze and K. K. Ng, *Physics of Semiconductor Devices* (Wiley, New York, 2007).
[7] J. E. Ortega and F. J. Himpsel, Phys. Rev. Lett. **69**, 844 (1992).
[8] Y. Jia, M. Özer, H. Weitering, and Z. Zhang, *Nanophenomena at Surfaces: Fundamentals of Exotic Condensed Matter Properties* (Springer, Berlin, 2011), Chap. Quantum Size Effects in the Growth and Properties of Ultrathin Metal Films, Alloys, and Related Low-Dimensional Structures, pp. 67–112.
[9] J. J. Paggel, T. Miller, and T.-C. Chiang, Science **283**, 1709 (1999).
[10] X. Ma, P. Jiang, Y. Qi, J. Jia, Y. Yang, W. Duan, W.-X. Li, X. Bao, S. B. Zhang, and Q.-K. Xue, Proc. Natl. Acad. Sci. U.S.A. **104**, 9204 (2007).
[11] A. Zhao, Q. Li, L. Chen, X. Xiang, W. Wang, S. Pan, B. Wang, X. Xiao, J. Yang, J. G. Hou, and Q. Zhu, Science **309**, 1542 (2005).
[12] T. Uchihashi, J. Zhang, J. Kröger, and R. Berndt, Phys. Rev. B **78**, 033402 (2008).
[13] V. Lindberg and B. Hellsing, J. Phys. Condens. Matter **17**, S1075 (2005).
[14] S. K. Hämäläinen, Z. Sun, M. P. Boneschanscher, A. Uppstu, M. Ijäs, A. Harju, D. Vanmaekelbergh, and P. Liljeroth, Phys. Rev. Lett. **107**, 236803 (2011).
[15] S.-h. Phark, J. Borme, A. L. Vanegas, M. Corbetta, D. Sander, and J. Kirschner, ACS Nano **5**, 8162 (2011).
[16] S. J. Altenburg, J. Kröger, T. O. Wehling, B. Sachs, A. I. Lichtenstein, and R. Berndt, Phys. Rev. Lett. **108**, 206805 (2012).
[17] D. Subramaniam, F. Libisch, Y. Li, C. Pauly, V. Geringer, R. Reiter, T. Mashoff, M. Liebmann, J. Burgdörfer, C. Busse, T. Michely, R. Mazzarello, M. Pratzer, and M. Morgenstern, Phys. Rev. Lett. **108**, 046801 (2012).
[18] W. Jolie, F. Craes, M. Petrović, N. Atodiresei, V. Caciuc, S. Blügel, M. Kralj, T. Michely, and C. Busse, Phys. Rev. B **89**, 155435 (2014).
[19] W. Jolie, F. Craes, and C. Busse, Phys. Rev. B **91**, 115419 (2015).
[20] N. Nilius, T. M. Wallis, and W. Ho, Science **297**, 1853 (2002).
[21] S. R. Schofield, P. Studer, C. F. Hirjibehedin, N. J. Curson, G. Aeppli, and D. R. Bowler, Nat. Commun. **4**, 1649 (2013).
[22] M. F. Crommie, C. P. Lutz, and D. M. Eigler, Science **262**, 218 (1993).
[23] L. Bürgi, O. Jeandupeux, A. Hirstein, H. Brune, and K. Kern, Phys. Rev. Lett. **81**, 5370 (1998).
[24] A. Mugarza, A. Mascaraque, V. Pérez-Dieste, V. Repain, S. Rousset, F. J. García de Abajo, and J. E. Ortega, Phys. Rev. Lett. **87**, 107601 (2001).
[25] J. Li, W. D. Schneider, R. Berndt, and S. Crampin, Phys. Rev. Lett. **80**, 3332 (1998).
[26] H. Oka, O. O. Brovko, M. Corbetta, V. S. Stepanyuk, D. Sander, and J. Kirschner, Rev. Mod. Phys. **86**, 1127 (2014).
[27] C. Tournier-Colletta, B. Kierren, Y. Fagot-Revurat, and D. Malterre, Phys. Rev. Lett. **104**, 016802 (2010).
[28] H. C. Manoharan, C. P. Lutz, and D. M. Eigler, Nature (London) **403**, 512 (2000).
[29] S. Crampin, H. Jensen, J. Kröger, L. Limot, and R. Berndt, Phys. Rev. B **72**, 035443 (2005).
[30] J. Kliewer, R. Berndt, and S. Crampin, New J. Phys. **3**, 22 (2001).
[31] H. Jensen, J. Kröger, R. Berndt, and S. Crampin, Phys. Rev. B **71**, 155417 (2005).
[32] J. Kröger, L. Limot, H. Jensen, R. Berndt, S. Crampin, and E. Pehlke, Prog. Surf. Sci. **80**, 26 (2005).
[33] J. Kröger, M. Becker, H. Jensen, Th. von Hofe, N. Néel, L. Limot, R. Berndt, S. Crampin, E. Pehlke, C. Corriol, V. M. Silkin, D. Sánchez-Portal, A. Arnau, E. V. Chulkov, and P. M. Echenique, Prog. Surf. Sci. **82**, 293 (2007).
[34] S. Crampin, M. H. Boon, and J. E. Inglesfield, Phys. Rev. Lett. **73**, 1015 (1994).
[35] S. M. Reimann and M. Manninen, Rev. Mod. Phys. **74**, 1283 (2002).
[36] M. Schmid, W. Hebenstreit, P. Varga, and S. Crampin, Phys. Rev. Lett. **76**, 2298 (1996).
[37] M. Schmid, S. Crampin, and P. Varga, J. Electron Spectrosc. Relat. Phenom. **109**, 71 (2000).
[38] O. Kurnosikov, H. J. M. Swagten, and B. Koopmans, Phys. Rev. Lett. **106**, 196803 (2011).
[39] O. Kurnosikov, J. H. Nietsch, M. Sicot, H. J. M. Swagten, and B. Koopmans, Phys. Rev. Lett. **102**, 066101 (2009).
[40] C. Sprodowski and K. Morgenstern, Phys. Rev. B **82**, 165444 (2010).
[41] O. Kurnosikov, D. V. Kulikov, V. S. Kharlamov, H. J. M. Swagten, and Yu. V. Trushin, Phys. Rev. B **84**, 054109 (2011).

[42] R. Otero, A. L. Vázquez de Parga, and R. Miranda, Phys. Rev. B **66**, 115401 (2002).
[43] M. Hupalo and M. C. Tringides, Phys. Rev. B **65**, 115406 (2002).
[44] M. Becker and R. Berndt, Phys. Rev. B **81**, 205438 (2010).
[45] I.-Po Hong, C. Brun, F. Patthey, I. Y. Sklyadneva, X. Zubizarreta, R. Heid, V. M. Silkin, P. M. Echenique, K. P. Bohnen, E. V. Chulkov, and W.-D. Schneider, Phys. Rev. B **80**, 081409 (2009).
[46] J. E. Inglesfield, *The Embedding Method for Electronic Structure* (Institute of Physics, Berkshire, 2015).
[47] M. Ziegler, N. Néel, A. Sperl, J. Kröger, and R. Berndt, Phys. Rev. B **80**, 125402 (2009).
[48] J. Li, W.-D. Schneider, S. Crampin, and R. Berndt, Surf. Sci. **422**, 95 (1999).